Improved electrochemical performance for high voltage spinel LiNi0.5Mn1.5O4 modified by supercritical fluid chemical deposition

Gwenaëlle Courbaron, Emmanuel Petit, Jon Serrano-Sevillano, Christine Labrugère-Sarroste, Jacob Olchowka, Dany Carlier, Nathalie Delpuech, Cyril Aymonier, Laurence Croguennec

Improved electrochemical performance for high voltage spinel $LiNi_{0.5}Mn_{1.5}O_4$ modified by supercritical fluid chemical deposition

Received 00th January 20xx,
Accepted 00th January 20xx

DOI: 10.1039/x0xx00000x

Gwenaëlle COURBARON[a,b], Emmanuel PETIT[a,c], Jon SERRANO-SEVILLANO[a,d,e], Christine LABRUGÈRE-SARROSTE[f], Jacob OLCHOWKA[a,c,d], Dany CARLIER[a,c,d], Nathalie DELPUECH[b,c,d], Cyril AYMONIER[a,c] * and Laurence CROGUENNEC[a,c,d] *

* corresponding authors : Laurence Croguennec (laurence.croguennec@icmcb.cnrs.fr) and Cyril Aymonier (cyril.aymonier@icmcb.cnrs.fr)

Abstract

Among candidates at the positive electrode of next generations of Li-ion technology and even beyond of post Li-ion technology as all solid-state batteries, spinel $LiNi_{0.5}Mn_{1.5}O_4$ (LNMO) is one of the favourite. Nevertheless, before its integration into commercial systems, challenges still remain to be tackled, especially the stabilization of interfaces with the electrolyte (liquid or solid) at high voltage. In this work, a simple, fast and cheap process is used to prepare a homogeneous coating of Al_2O_3-type to modify the surface of the spinel LNMO: the supercritical fluid chemical deposition (SFCD) route. This process is, to our knowledge, used for the first time in the battery field. Significantly improved performance was demonstrated versus those of bare LNMO, especially at high rates and for highly loaded electrodes.

KEYWORDS: Lithium-ion batteries, surface modification, high voltage positive electrode material, spinel oxide $LiNi_{0.5}Mn_{1.5}O_4$, Supercritical Fluid Chemical Deposition

INTRODUCTION

One of the most important source of greenhouse gas emission is transportation due to fossil fuel dependency. The use of lithium-ion (Li-ion) batteries and more widely electrochemical energy storage systems are great opportunities for decreasing global environmental footprint with the development of electrical and hybrid vehicles, especially if these batteries are powered with renewable energies. SONY developed the first Li-ion battery technology in 1991 and since then Li-ion batteries have become the main electrochemical energy storage system for mobile phone and electronic devices[1], and more recently, for transportation and storage of intermittent renewable energies[2]. However, the electric vehicles (EVs) market requires cheaper batteries with more autonomy, faster charge rates, longer cycle life and improved safety. Thus, it implies the development of Li-ion batteries with higher energy and power densities. Nowadays, this technology is close to its limitations in terms of cells gravimetric and volumetric energy densities (~300 Wh/kg and ~700 Wh/l, respectively) with graphite at the negative electrode and layered oxides of general composition $LiMO_2$ at the positive electrode ($LiNi_{1-x-y}Co_xAl_yO_2$ (NCA) or $LiNi_{1-x-y}Mn_xCo_yO_2$ (NMC))[3-4]. Perspectives to increase the energy density are the use of alternative positive electrode materials with redox reactions occurring at higher voltages, or showing the activation of multi-electron reactions or of combined anionic and cationic redox reactions[5]. The cobalt-free $LiNi_{0.5}Mn_{1.5}O_4$ (LNMO) spinel oxide looks promising as a high voltage positive electrode material with the activation of the redox couples $Ni^{2+}/Ni^{3+}/Ni^{4+}$ at 4.7 V vs. Li^+/Li (a two-electron reaction), a three dimensional pathway for Li^+ ions, and a high energy density of 650 Wh/kg at the chemistry level. Furthermore, this compound is cobalt-free. Indeed, beyond that the use of cobalt is controversial as its extraction is mainly done in Democratic Republic of Congo by children under non-human rights conditions, its substitution is required as Co is in the list of critical elements. In addition the price of Co is very high (72000 USD/t in June 2022).[6] However, some issues have to be mentioned, such as (i) promotion of electrolyte decomposition at high voltages (> 4.9 V vs. Li^+/Li) and (ii) Mn^{2+} dissolution at the interface with the electrolyte which is detrimental for the cyclability of the battery due to crosstalk between the two electrodes[7,8]. To solve these problems, two main approaches are investigated: i) the development of new electrolyte formulations with stabilizing additives[9–11] or ii) the surface modification of the positive electrode material in order to stabilize the Cathode Electrolyte Interface (CEI) and improve the cyclability. The second approach is the one developed in this work.

Different inorganic materials can be used as surface coating layers, such as oxides (Al_2O_3, SiO_2, $LiAlO_2$, $Li_4Ti_5O_{12}$, Li_2SiO_3, etc.)[12–19], fluorides (AlF_3, LaF_3, etc.)[20–22], or lithium-conducting solid electrolytes ($Li_{1.3}Al_{0.3}Ti_{1.7}(PO_4)_3$, etc.)[23,24]. The low cost and abundant Al-rich oxide Al_2O_3 was selected in this study. In addition to its economic advantages, Al_2O_3 could act as a HF scavenger.[25–27] It would transform HF generated from the electrolyte decomposition, to form a metal fluoride (AlF_3) by scavenging F^- from the HF. The AlF_3 surface layer as formed protects then the active material from further HF attack. One of

a Univ. Bordeaux, CNRS, Bordeaux INP, ICMCB, UMR 5026, F-33600 Pessac, France
b Renault SAS, Technocentre, 1 avenue du golf, 78280 Guyancourt, France
c RS2E, Réseau Français sur le Stockage Electrochimique de l'Energie, FR CNRS 3459, France
d ALISTORE-ERI European Research Institute, FR CNRS 3104, 80039 Amiens Cedex France
e Centro de Investigación Cooperativa de Energías Alternativas (CIC energiGUNE), Basque Research and Technology Alliance (BRTA), Parque Tecnológico de Álava, Albert Einstein 48, 01510 Vitoria-Gasteiz, España.
f PLACAMAT, UAR 3626, CNRS Université Bordeaux, 33600 Pessac, France

the most commonly techniques used to prepare an Al_2O_3 coating is the atomic layer deposition (ALD),[12,28–32] which allows a fine tuning of the thickness. Nevertheless, up to now ALD is mainly performed directly on electrodes and not on powders due to difficulties to control the formation of a homogenous coating without any flow (fluidisation) of particles. The drawback in that case could be a loss of percolation with the generation of a coating of the conductive additive and binder together with the positive electrode material, and thus a loss of electrochemical performance especially at high rates. Moreover, for future battery technology such as all-solid-state batteries, different chemistries of coatings could be required at each interface between the electrode materials and the electrolyte. The ALD technique appears as non-flexible enough to develop coatings on demand, as this process is expensive, difficult to up-scale at the industrial level and with a rather slow deposition rate[33]. More classical methods such as sol-gel or coprecipitation have also been reported to prepare Al_2O_3 coating,[34–36] but a thermal treatment is often required to fully decompose the precursors and remove all the residual groups such as hydroxyls at the surface.[14,15] Additionally, high temperature sintering (> 500 °C) often leads to interdiffusion between the coating layer and the active material and to possible decrease of electrochemical performance. The control of the homogeneity and thickness of the coating is critical, in order to well balance the improved cyclability versus the increase of the interfacial resistance. Here, we report a new route to protect the surface of these high voltage spinel oxides: supercritical fluid chemical deposition (SFCD) method which has proven to be efficient to prepare homogeneous covering layers of controlled thicknesses.[37] The use of supercritical fluids (SCFs) permits to reach interesting hybrid thermophysical properties[38]. Indeed, SCFs exhibit gas-like viscosities and diffusivities while they have a liquid-like densities. This property helps for the dissolution of metallic precursors especially for chemical deposition. It is an emerging method to modify material surfaces, never reported in the field of battery materials. The main advantages compared to common coating techniques are[38]: i) the use of a green solvent[39] (mainly CO_2) compared to other techniques (CVD, ALD[40]), ii) the reduced deposition time (deposition rate in SFCD is more than one order of magnitude higher than in ALD), iii) the access to a wide range of coating compositions[41], iv) the dry and ready-to-use coated powder after the SFCD method and v) the possible scale up of the process (possibility of a continuous process). The surface-modified LNMO spinel oxides will be characterized combining diffraction, microscopy and spectroscopy experiments in order to determine, for highly loaded positive electrodes, the relationship between the characteristics of the alumina-based coating and the electrochemical performance in Li-ion batteries cycled at high rates.

EXPERIMENTAL SECTION

Surface modification processes

LNMO powder was received from Nano One Materials Corp, stored under ambient air and presents a mass-median-diameter d_{50} of 16 µm and a specific surface area S_{BET} of 0.96 m²/g. Aluminium acetylacetonate ($Al(C_5H_7O_2)_3$ ($Al(acac)_3$) from ACROS ORGANICS (97%)) dissolved in absolute ethanol was used as Al precursor for the preparation of the Al_2O_3-type layer at the LNMO surface.

Two different synthesis routes were used, to prepare Al-rich modified LNMO samples. The first method used as reference is the dispersion. For 1 mol.% of Al_2O_3 theoretically expected compared with LNMO material, 35.5 mg of $Al(acac)_3$ were dissolved at 40 °C into 30 mL of absolute ethanol under stirring into an Erlenmeyer flask, before adding the LNMO powder (1 g). The pH was adjusted with NH_3 base until 12, and then stirred for one night (12h). This step will help to form $Al(OH)_3$ particles from the degradation of $Al(acac)_3$, those being reactive with LNMO surface thanks to hydroxyl groups. Solvents, ethanol and NH_3, were evaporated at 55°C under vacuum using a rotavapor. Finally, the powder recovered was heat treated in a tubular furnace at 260°C for 2h under air to finally decompose the aluminium phase into an amorphous phase (The thermogravimetric analysis of the acac precursor is given in supplementary information in **Figure S1**). The series of samples as obtained are called DIS 0.5%, DIS 1%, DIS 2.5%, DIS 5%, and DIS 10% in the following discussion as prepared with 0.5, 1, 2.5, 5 and 10 mol.% ratios theoretically expected compared with LNMO material. For comparison, a blank was also prepared: LNMO powder was dispersed, without acac, in absolute ethanol at pH 12 during one night (12h) before being thermally treated at 260 °C for 2h. SFCD was also used to modify the LNMO surface (Erreur ! Source du renvoi introuvable.). The same suspension (LNMO/Acac/Ethanol) is prepared but without NH_3 because in the case of SFCD, $Al(acac)_3$ is soluble in the mixture ethanol/CO_2. The mixture was stirred continuously during one night (12h) before being poured into a 50 mL high pressure and high temperature vessel reactor, which was filled with CO_2 gas at 5 MPa. CO_2 was chosen as the main reaction solvent for its easily accessible critical pressure and temperature (Pc = 7.38 MPa and Tc = 31 °C) and the possibility to remove it (recycle it at larger scale) for recovering a dry coated powder, ready to use. Absolute ethanol was chosen as co-solvent in order to increase the solubility of the metal precursor. The reactor was heated up to 170 °C (at ~10 °C/min) and maintained under stirring with a speed of 500 rpm. When temperature rises, pressure increases inside the reactor to reach around 10 MPa once the temperature is stabilized. Then, compressed CO_2 was added until a pressure of 20 MPa was obtained. Under these conditions, the mixture CO_2/ethanol (molar composition 80:20) is supercritical. Indeed, the critical pressure and temperature of this mixture are P_c = 14.5 MPa and T_c = 92 °C, respectively[42]. The use of these conditions allows the decomposition of the precursor and then the deposition of an Al-rich coating layer at the surface of the active material. After one hour of reaction at 20 MPa and 170 °C, the powder was dried by removing the solvent using a continuous CO_2 flow. Then, the reactor was cooled down and depressurized, and the dry coated LNMO was recovered. The series of samples as obtained was called SFCD 0.1%, SFCD 0.5%, SFCD 1%, SFCD 2.5%, SFCD 5% and SFCD 10%, when modified using 0.1%, 0.5%, 1%, 2.5%, 5% and 10 mol.% ratios of Al_2O_3 theoretically expected compared with LNMO material, respectively.

Considering the formation of a homogeneous coating at the surface of LNMO particles as Al_2O_3, thicknesses of 0.6, 3, 6, 15, 30 and 60 nm are expected for 0.1%, 0.5%, 1%, 2.5%, 5% and 10 mol.% of Al_2O_3, respectively. These values have been calculated considering the specific surface of the spinel (0.96 m^2/g) and taking into account densities for LNMO and for Al_2O_3 of 4.44 g/cm^3 and 3.95 g/cm^3, respectively.

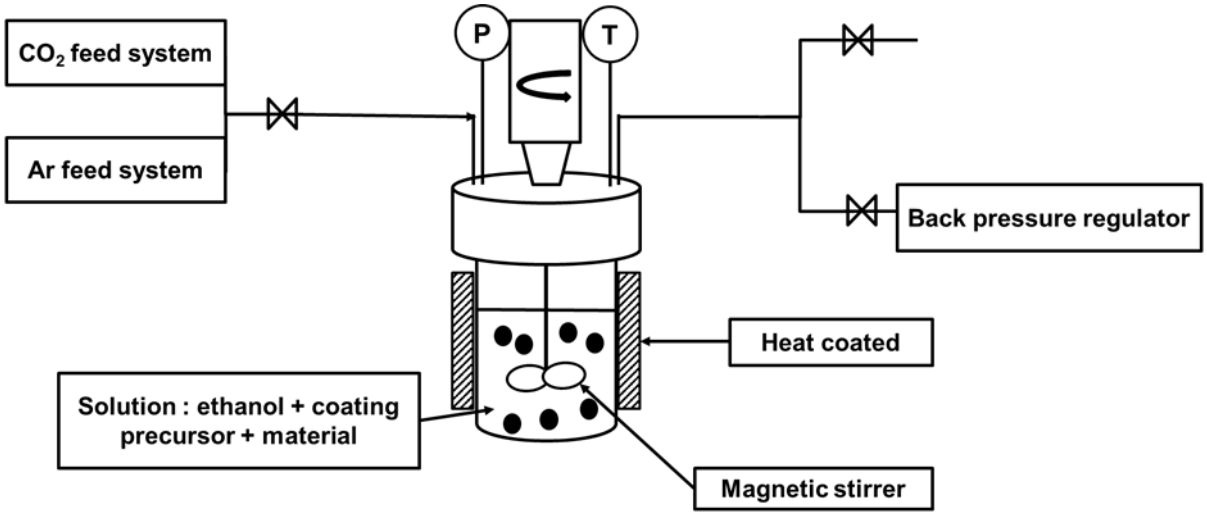

Figure 1 : Scheme of the SFCD process.

Electrode preparation, cell assembly and electrochemical tests

85 wt.% LNMO powders, bare or coated, were mixed with 10 wt.% conductive carbon (Alfa Aesar, 99.9%) and 5 wt.% polyvinylidene fluoride (PVDF, Sigma Aldrich) in N-methyl-2-pyrrolidone as solvent (NMP, Sigma Aldrich, 99.5%). The mixture was stirred at 900 rpm during at least 2 h at ambient temperature to obtain a homogeneous slurry. Then, this slurry was casted with a thickness between 130 and 500 µm, depending on the mass loading expected, on a 50 µm thick aluminium foil. To remove NMP, the resulting wet electrode is placed in an oven at 80 °C overnight (12 h), 16 mm diameter electrode disks were cut and calendared under a press at 5 tons to reduce porosity down to 40%. Once dried during one night at 80 °C under vacuum, electrodes and separators were placed into an Ar-filled glovebox (with H_2O and O_2 contents lower than 1 ppm). Li metal was used as counter electrode. The electrolyte (Solvionic, 99.9 % - 20 ppm max H_2O) was 1M $LiPF_6$ dissolved in ethylene carbonate and dimethyl carbonate (EC-DMC) (with a 1:1 v:v ratio). The electrochemical performance was evaluated via a Biologic test system in the potential range of 3.5-4.9 V vs Li^+/Li. Rate capability (1C = 0.5 mA/cm^2) and endurance tests have been done considering 1C = 135 mAh/g_{LNMO}. For the coated materials, the obtained capacity is given taking into account the mass of the active material (LNMO) and the mass of the coating.

Material characterization

The X-ray powder diffraction patterns were collected using a PANalytical X'pert PRO MPD diffractometer in Bragg Brentano θ-θ geometry equipped with a secondary monochromator and X'celerator multi-strip detector. Each measurement was made within an angular range of 2θ = 8-80 ° and lasted for 34 minutes. The Cu Kα radiation (λ=1.5418 Å) was generated at 45 kV and 40 mA. XRD was used to identify the phases, compare the crystallinity and structural parameters of as-prepared materials. The Fullprof suite[43] was used to perform Le Bail (profile and cell parameters) refinements.

Chemical analyses were performed by Inductively Coupled Plasma – Optical Emission Spectrometry (ICP-OES) (Varian ICP-OES 720 ES) to quantify the Mn and Ni amount in the material. Coated and uncoated materials (12-15 mg) were dissolved into an acidic mixture made of 2 mL $HClO_4$, 4 mL HF, 4 mL HNO_3 and 4 mL H_2SO_4 and poured into a Teflon reactor before being introduced into a microwave at 180 °C (Heating rate: 12 °C/min, natural cooling in less than 1 h) during 30 min to dissolve all the powders. In order to ensure reproducibility, each sample was prepared twice and each solution was measured 5 times. The results of these titrations are given in **Table S1**.

High-resolution scanning electron microscopy (HR-SEM) images were collected on a JEOL JSM-6700F microscope to check the morphology and surface modifications, and energy dispersive spectroscopy analyses (EDS, Tescan Vega Compact) were performed to determine changes in composition of the as-prepared materials with a 15 keV acceleration voltage.

Solid-state nuclear magnetic resonance (ssNMR) technique was used to study the local atomic and electronic environment of the probed nucleus, here ^{27}Al and ^{7}Li and to highlight the presence of aluminium at the surface of the material considering the general shape of the integrated signal as the interaction varies according to $1/r^3$, r being the distance in space between the probed diamagnetic nucleus and the electronic spins of the paramagnetic material, here LNMO. ^{7}Li solid-state NMR experiments were performed on a Bruker Advance III 100 MHz (2.35 T) spectrometer equipped with a 2.5 mm MAS probe. A rotor-synchronized Hahn echo (π/2 - τ - π) sequence was used with a π/2 pulse length of 1.1 µs and a recycle delay of 0.5 s, and 96000 scans were acquired. The spectra were calibrated to a 1 M solution of LiCl. ^{27}Al ssNMR experiments were performed on

a Bruker Advance III 300 MHz (4.69 T) spectrometer equipped with a 2.5 mm MAS probe. A one pulse sequence was used with a pulse length of 1.16 µs and a recycle delay of 0.5 s. All samples were prepared in air and spinning frequencies were set to 30 kHz.

Raman spectra were collected with a confocal LabRAM HR Evolution microspectrometer from Horiba equipped with a 633 nm argon ion laser. They were collected in the wavenumber range of 100 - 800 cm^{-1}, using a 10.6 mm focal length lens and an acquisition time of 10 s and 20 accumulations.

Fourier Transformed Infrared (FT-IR) spectroscopy was performed on a Bruker Equinox 55 spectrometer in the wavenumber range of 400 - 4000 cm^{-1} with a resolution of 4 cm^{-1}. Samples were grounded in a mortar with dried KBr (120 °C), in an approximate ratio of 3/50 (by wt.%) and until a homogeneous mixture was obtained. The background was made before each series of analyses and automatically subtracted from each spectra to remove H_2O and CO_2 traces. The spectra were collected with OPUS software.

Transmission electron microscopy (TEM) was performed on a TEM-HR JEOL 2200FS 200 kV microscope. EDS was also carried out by mapping to check for the repartition of the different elements. Two drops of a suspension made of powder in absolute ethanol were deposited onto a copper grid with carbon membrane, prepared for TEM-EDS observation.

Auger electron spectroscopy (AES) was performed using a PHI 710Xi Auger nanoprobe equipped with a cylindrical mirror analyser (CMA) mounted coaxially with respect to the electron column. Thanks to this particular system geometry, the take-off angle of the analysed Auger electrons is below 30 ° from the primary electron beam and thus permits to avoid shadowing effect. The pressure in the analysis chamber was maintained between 10^{-10} and 10^{-9} mbar. The electron beam was set normal to the surface, at 10 keV accelerating energy and 10 nA current to obtain approximately 20 nm spot size. Specific zones of a few micron-square were selected for scanning and spectra acquisition in order to optimize the signal intensity to noise ratio and limit the charge effect of the surface. Spectra were acquired in direct mode with a step size of 3 eV. AES allows an information about the thickness of the coating thanks to stripping on few nanometers.

A ThermoFisher Scientific K-ALPHA spectrometer was used for XPS surface analysis with a monochromatized Al-Kα source (hv = 1486.6 eV) and a 400 µm X-Ray spot size. Powders were pressed onto indium foils. The full spectra (0-1350 eV) were obtained with a constant pass energy of 200 eV, while high-resolution spectra were recorded with a constant pass energy of 40 eV. Charge neutralisation was applied during the analysis and depth profiles were fulfilled with an Ar^+ ion gun. High resolution spectra (i.e., C1s, O1s, Li1s, Mn2p, Ni2p, Al2p …) were quantified using the Avantage software provided by ThermoFisher Scientific. Main attention was paid on Al 2p, O 1s, C 1s fittings after energy shift of all spectra compared to C 1s maximum peak at around 284.8 eV. The spectra of the different samples were obtained in the same conditions so it is possible to compare them directly.

RESULTS AND DISCUSSION

Structure and morphology of the modified LNMO samples

XRD patterns were collected for each coated material, either obtained by the dispersion method followed by a thermal treatment, or obtained by the supercritical fluid-based process. The patterns obtained for the series of coated samples are very similar to that of the pristine one, given as reference in Erreur ! Source du renvoi introuvable.. They exhibit diffraction peaks typical of a spinel type phase, described in the *Fd-3m* space group (JCPDS N°80-2162), and the sharpness of the peaks indicates good crystallinity with crystalline domains bigger than 1 µm ($FWHM_{(111)}$ = 0.1154(3) °. Moreover, whatever the sample, no extra peaks are observed for the coated materials suggesting either that, the material is not modified at all, or that the aluminium-rich phase formed during the coating process is amorphous in both cases. Indeed, Le Bail refinements of XRD patterns for the bare LNMO and for the two 10 mol.% modified LNMO lead to very similar cell parameters and volumes, ranging between 8.1714(4) and 8.1722(4) Å and between 545.61(5) and 545.81(5) $Å^3$, respectively **(Figures S2** and **Table S2)**. From these first results, it appears thus, that the structure of the bulk LNMO was not modified in contact with the supercritical CO_2/EtOH mixture. Reference materials were prepared from the decomposition of $Al(acac)_3$ alone in the conditions used for the formation of the coatings, in order to compare them with those formed on or next to LNMO particles. **Figures S3a-b** show their XRD patterns. Surprisingly, the material obtained by the dispersion process is crystalline and contains a large amount of the acac precursor, whereas the material obtained by the supercritical fluid-based process is amorphous, revealing only three broad lines at 18 °, 25 ° and 40 ° (2θ). In the former case,

a better degradation of the precursor is thus observed in contact with LNMO, as no residue of $Al(acac)_3$ is observed. Another main difference is observed between the two processes: the first is done in a closed environment and allows thus the control of the Al content in the final powder, whereas in the case of the dispersion process the system is open making that part of $Al(acac)_3$ precursor could be lost, as volatile, during the thermal treatment.

The morphology and surfaces of the pristine and Al-rich coated LNMO materials have been investigated by HR-SEM. As observed in Erreur ! Source du renvoi introuvable., all the samples are characterized as expected by octahedral shaped

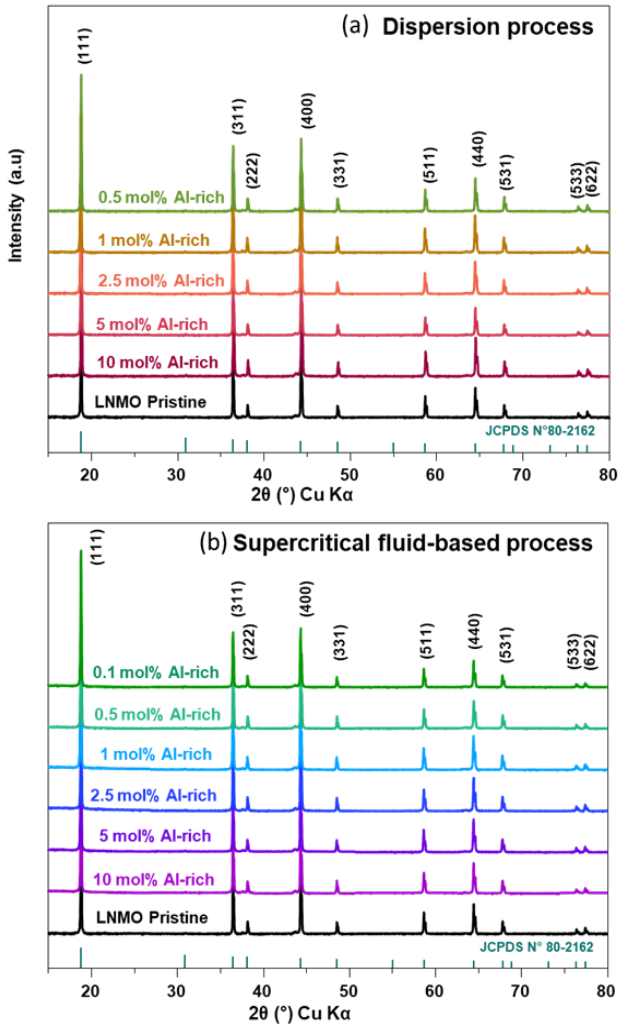

Figure 2 : XRD patterns of the pristine and coated LNMO samples obtained either by a dispersion process followed by a thermal treatment (a) and by a supercritical fluid-based process (b).

particles[44]. Pristine LNMO shows smooth surfaces with sharp edges (**Figures 3a-b**), whereas a coating is obviously observed at the surface of both modified LNMO with softened edges (Erreur ! Source du renvoi introuvable.**c-f**). Moreover, in the case of the SFCD modified material, the surface layer seems to be more homogeneous and covering than the one obtained by dispersion. Indeed, for the latter, small aggregates and roughness are observed in Erreur ! Source du renvoi introuvable.**c**, and even better in Erreur ! Source du renvoi introuvable.**d**.

Surface modification appears not detectable by XRD and has no impact on the lattice parameters or the initial morphology of the spinel material. However, the formation of the coating layer is clearly observed at the surface of LNMO by HR-SEM, as an amorphous phase.

Surface characterization of modified LNMO samples

In order to characterize deeper the modification of LNMO powder, ^{7}Li and ^{27}Al solid state MAS NMR experiments were performed. The ^{7}Li MAS NMR spectra collected for pristine and coated materials are similar, as shown in **Figure S4** in supplementary information, which means that local environment of lithium remains unchanged after the formation of the coating in good agreement with no modification of the bulk of LNMO as supported by XRD. **Figure 4** compares the ^{27}Al

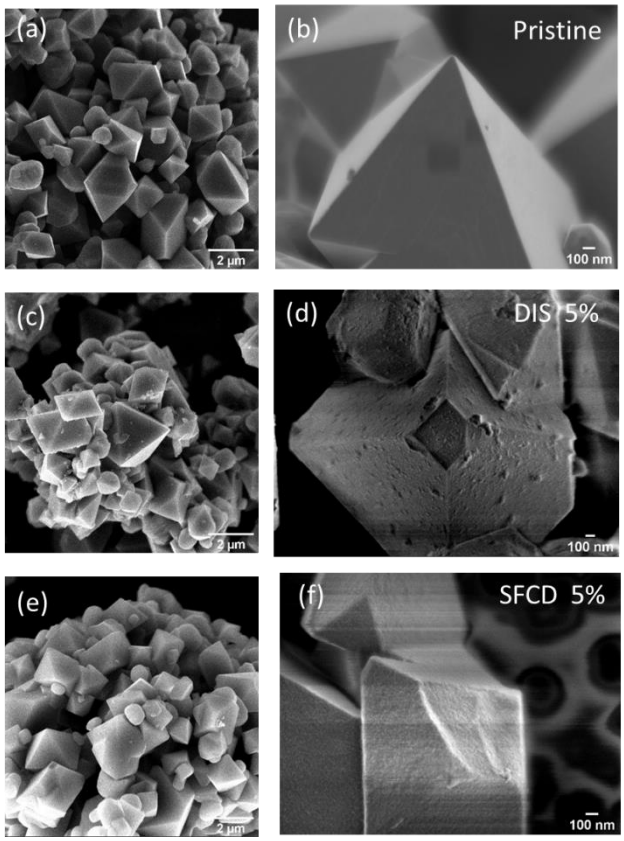

Figure 3 : SEM and HR-SEM images of pristine LNMO (a-b) and 5 mol. % Al_2O_3 theoretically expected modified LNMO obtained by the dispersion process (c-d) and by the supercritical fluid-based process (e-f).

MAS NMR spectra of aluminium phase prepared as reference by SFCD and of three modified LNMO samples prepared either by different processes or with different amounts of coating. Three local environments are observed for aluminium in each case. The most intense peak at around 2 ppm is assigned to AlO_6 environment, the one at 31 ppm to AlO_5 and the one at 61 ppm to AlO_4 environment[45]. First, as shown by the difference of

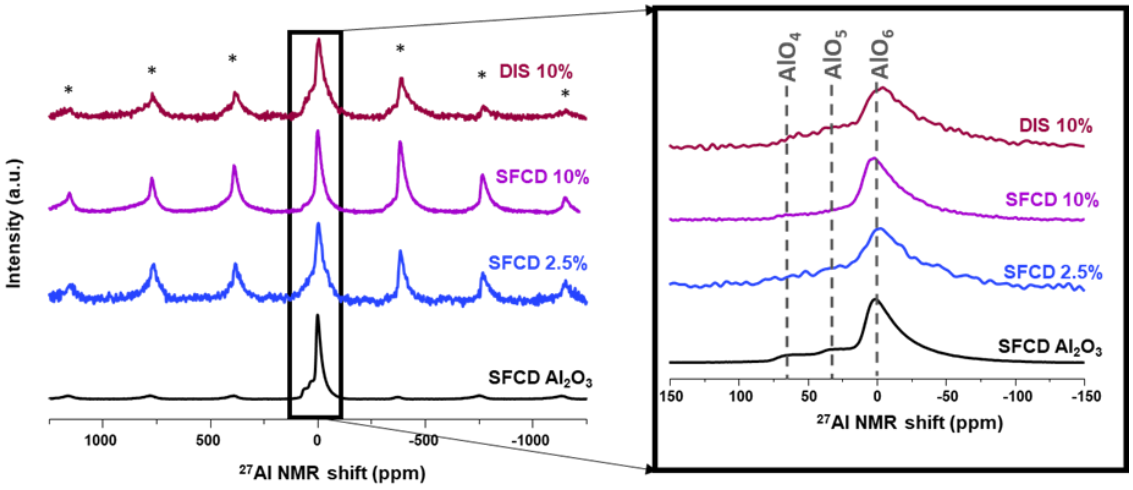

Figure 4 : ^{27}Al MAS NMR spectra (300 MHz, 30 kHz) of LNMO materials coated using SFCD and dispersion processes and bare aluminium phase prepared by SFCD as reference. Spinning sidebands are denoted with asterisks.

spectra given in **Figure S5** and by the similarity of those given in **Figure 4**, the DIS and SFCD processes used to modify LNMO allow the transformation of the aluminium acetylacetonate precursor into a similar phase which appears amorphous as not detected by XRD whatever its content. The shape and the relative intensities of the observed signals are well consistent with those reported in literature for an amorphous alumina phase[45], with the presence of AlO_6 and AlO_4 peaks[46]. The narrowness of the AlO_6 peak suggests an increase in topological order in the amorphous oxide with the presence of small crystalline domains[47]. On the contrary, the presence of the AlO_5 signal is directly linked to a structural disorder and corresponds to coordination defects and indicates the presence of amorphous structure [48].

Paramagnetic materials can induce dipolar interactions with the nucleus close by, with a fast intensity decay with the mean distance ($1/r^3$) between the electron spin and the probed nucleus. This leads to an overall broadening of the lineshape, but this effect will only be felt by the closest neighbours. This means, that the extension and the intensity of the spinning sidebands will provide an idea of the proximity between the coating and the LNMO.

As expected, the NMR spectrum collected for a less coated material (2.5 % versus 10 %) shows a worst signal-over-to-noise ratio, but a similar shape for the isotropic signals with their spinning sidebands. The large broadening of the global NMR signal and the large number of spinning sidebands reveal the spatial proximity of the ^{27}Al probe nucleus to the paramagnetic transition metals containing material (here mainly Ni^{2+} (d^8 $t2g^6eg^2$) and Mn^{4+} (d^3 $t2g^3$)), but as confirmed by Raman spectroscopy without any diffusion of Al into the spinel structure (**Figure S6**). This shape of the NMR signal envelope proves a high proximity between the coating and the LNMO particles, in agreement with the formation of a coating as thin layer. In the case of the dispersion process, for the same theoretical amount of coating (10 %) the NMR signal normalized to the acquisition time (**Figure S7**) is less intense, suggesting a smaller amount of coating formed than expected. The semi-quantitative analysis allows estimating 13 % for SFCD 10 % and 10 % for DIS 10 %. The order of magnitude is the one expected, showing furthermore that SFCD 10% has a bigger amount of AL-rich material at the surface than DIS 10%.

As shown on FT-IR spectra displayed in **Figure 5** and **Figure S8**, the surface modified LNMO samples do not contain any residue of acac precursor. The spectrum of each coated material contains all the peaks characteristic of the bare LNMO material showing a disordered structure described the *Fd-3m* space group,[49] whereas the additional peaks observed above 800 cm^{-1} are similar to those typical of the coating prepared in supercritical conditions as reference. The bands observed at 1030 and 860 cm^{-1} and attributed respectively to vibrations of Al=O and Al-O are characteristic of an Al_2O_3-type phase[50]. Nevertheless, signals corresponding to vibrations of O-H, C-H and C=C groups are also detected at 3550 cm^{-1}, 2968 and 2930 cm^{-1}, and around 1600-1500 cm^{-1}, respectively (**Figure S8**). These results suggest that an aluminium rich (oxyhydr)oxide amorphous coating is formed with residues of carbon coming from the transformation of $Al(acac)_3$[51]. Finally, as expected, the larger the coating content, the more intense are its related peaks. **Table S3** summarizes wavenumbers and assignment for the different peaks observed.

TEM-EDS analysis was performed in order to determine the aluminium distribution within the powder. The results obtained for the sample SFCD 10 % are given as an example in Erreur !

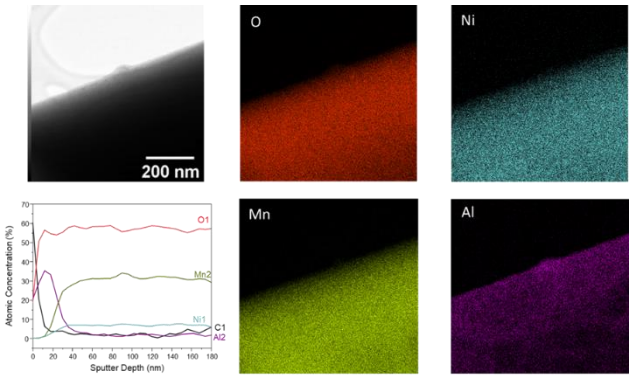

Figure 5 : TEM-EDS mapping of surface coated material SFCD 10% showing O, Ni, Mn, and Al repartition in red, blue, green and purple, respectively. and Nano Auger spectra of SFCD 10%.

Source du renvoi introuvable.. They show that a homogeneous Al-rich coating is formed at the surface of LNMO whose thickness was estimated to be 15 – 20 nm by nano Auger spectroscopy, which is less than expected. Indeed, the estimation predicted a theoretical thickness of 60 nm if all the particles were homogeneously covered. The synthesis being done in a closed reactor, the organic part of the acac precursor after its transformation can interact with the coating surface and stop the growth; this can explain the difference between the theoretical and experimental thicknesses. Thicker coating being not necessary for such battery application, this has not been optimized in this study.

XPS, as a surface characterization technique probing 5 to 10 nm in depth, allowed determining the covering of LNMO by the Al-rich coating, as well as the nature of chemical elements (chemical bonds and oxidation states) present at the extreme surface. The corresponding survey XPS spectra are given in **Figure S9** for the bare and coated LNMO materials, as well as for the coating prepared as reference in SCFD conditions. Erreur ! Source du renvoi introuvable. shows the Mn 2p, Ni 2p and Li 1s XPS spectra. Two main peaks are observed at 654.1 and 642.3 eV in all the Mn 2p spectra; they correspond to the tetravalent manganese associated to Mn $2p_{1/2}$ and Mn $2p_{3/2}$ spin-orbit coupling components, respectively[52]. The Li 1s peak is at 53.9 eV, while two peaks are observed at 854.7and 861.1 eV[53], the main peak $2p_{3/2}$ and its satellite being associated to divalent nickel in environment close to that observed in $Ni(OH)_2$ [54]. The absolute intensity of these peaks associated to LNMO decreases with an increasing covering of the surface by the Al-rich coating. These results reveal that the modified SFCD 2.5 % sample is more covered than the DIS 2.5 % sample, and, as expected, itself even more than the bare LNMO. It demonstrates that the SFCD process allows preparing more covering coatings than the dispersion process.

The O 1s, Al 2p and C 1s spectra of bare LNMO, SFCD 2.5 %, DIS 2.5 % as well as the SFCD Al-rich coating are compared in Erreur ! Source du renvoi introuvable.**a-n**. The fitted spectra are also given for information to identify better the nature of the coating. The assignment of each contribution is reported in **Table S4**. **Figure 8a-c** fully supports the results reported in **Figure 7**. Indeed, the surface modified LNMO by SCFD appears much more covered as its characteristic XPS spectra are close to those of the Al-rich coating alone, whereas those characteristic of the DIS 2.5 % material are intermediate between those of the bare LNMO and the coating alone. For the O 1s core level (**Figure 8d**), bare LNMO shows a main contribution at 529.7 eV associated to M-O bonds in LNMO (M = Ni, Mn). Minor contributions at 530.7, 531.6 and 533.0 eV could be attributed to C=O and C-O[55], but also to OH bonds and adsorbed water[56], respectively. Carbon pollution is at the origin of some of these peaks. The O 1s spectrum of the coating

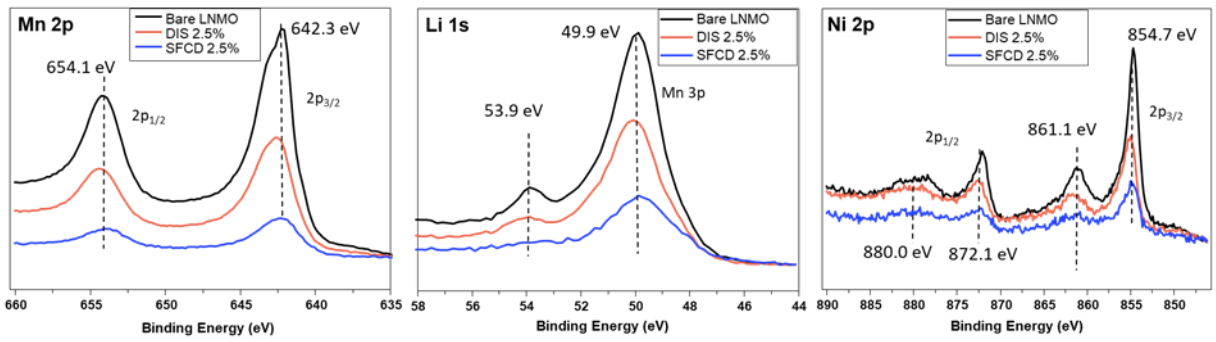

Figure 6 : Mn 2p, Li 1s and Ni 2p XPS spectra of bare and coated LNMO samples.

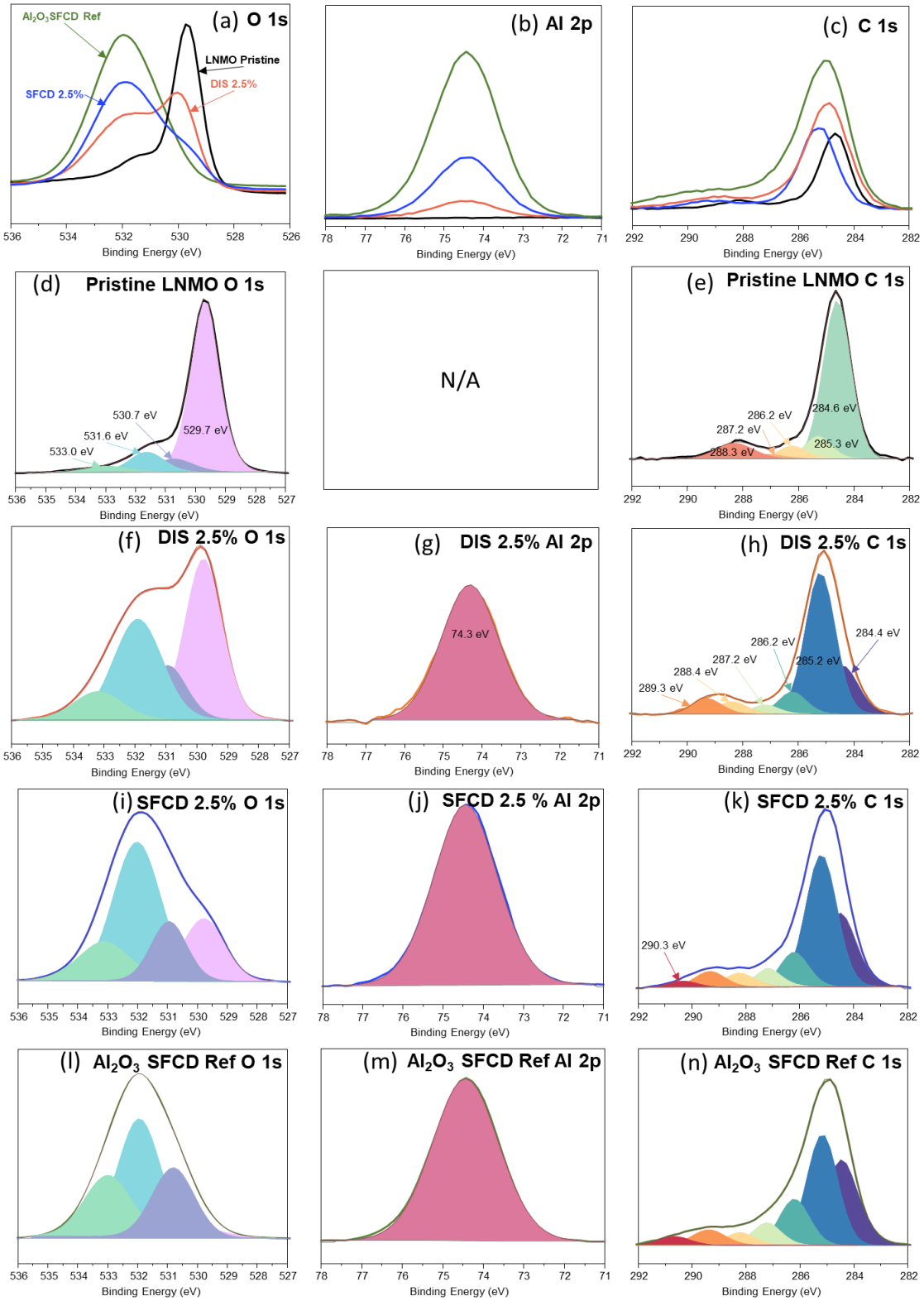

Figure 7 : O 1s, Al 2p and C 1s XPS spectra for bare LNMO (black line), 2.5 mol. % DIS (orange line) and SFCD (blue line) coated, as well as Al_2O_3 SFCD Ref (green line): inter-comparisons in (a), (b) and (c), fitted spectra in (d-n). The different contributions to a spectrum associated to an element are highlighted by different colours.

material prepared as reference in SFCD conditions shows only three contributions with the most intense at 531.9 eV. This one is attributed to Al-O bonding energies[55], while the others could correspond to C-O type bonds but also O-H type bonds as it is highlighted in FT-IR. In the case of the coated LNMO materials (SFCD 2.5 % and DIS 2.5 %), the ratio of intensities between the O 1s peak at 529.8 eV (Mn-O, Ni-O) and the one at 531.9 eV (Al-O) appears significantly dependant on the process used, and is thus a very good criterion to determine the efficiency of the process to prepare a covering coating: the higher the ratio, the less covered is the active material (Erreur ! Source du renvoi

introuvable.**a)**. This ratio is 0.54 for the SFCD 2.5 % material versus 1.25 for the DIS 2.5 %
material, showing for the former a better covering by the Al-rich coating. This trend is supported by changes in intensity for the Al 2p core level peak at 74.3 eV which corresponds also to Al-O bonds **(**Erreur ! Source du renvoi introuvable.**b)**. Its intensity is null for the base LNMO material (as expected) and increases for the DIS 2.5 %, SFCD 2.5 % and coating alone materials. Fitted C 1s spectra allow to determine that residues of carbon remain within the coating after the aluminium precursor transformation. Indeed, the C 1s spectrum of the bare LNMO exhibits five contributions at 284.6, 285.3, 286.2, 287.2 and 288.3 eV, which correspond to CHx, C-CO, C-O, C=O and COOR, respectively[57]. These contributions are due to carbon pollution at the surface of LNMO. The analysis of the coating material C 1s spectrum requires an additional contribution at low energy (~284.4 eV), suggesting the presence of C-C aromatic for both coated materials. Moreover, for SFCD material, a 290.3 eV component is revealed probably linked to some CF_2 bonding coming from the O-ring.

Atomic concentrations of Mn, Ni, Al and O, determined by the quantitative analysis of the XPS spectra, are summarized in Erreur ! Source du renvoi introuvable. for each sample. Mn/Ni ratios were calculated in order to check for changes in surface composition before and after coating. Bare LNMO material exhibits a Mn/Ni ratio at its surface equal to 4, as well as the coated materials. For "Al_2O_3 SCFD reference" the ratio O/Al is 1.33, i.e. lower than that expected for Al_2O_3 (O/Al = 1.5) but closer than that for others possible Al rich material as $Al(OH)_3$ where O/Al is equal to 3. This ratio is equal to 1.49 and 1.85 for the SFCD 2.5 % and DIS 2.5 % materials, respectively, suggesting a composition for the coating close to Al_2O_3 for the former and enriched in hydroxyl groups for the latter. Finally, the ratio of Al/(Ni+Mn) clearly shows that SFCD process allows the formation of a more covering coating, by five times (5.71 vs. 1.03), than the dispersion process.

Table 1 : Surface Mn, Ni, Al and O atomic concentrations extracted from the global analyses of XPS spectra and comparison of O/Al and (Al/(Ni+Mn)) intensity ratios.

	Atomic concentrations				Ratios		
	Mn	*Ni*	*Al*	*O (Al-O)*	*Mn/Ni*	*O/Al*	*Al/(Ni+Mn)*
Pristine	13.8	3. 3	N/A	N/A	4.2	N/A	N/A
DIS 2.5%	7.1	1.6	9.0	16.6	4.4	1.8	1.0
SFCD 2.5%	2.2	0.6	15.6	23.2	3.8	1.5	5.7
« Al_2O_3 SFCD »	N/A	N/A	17.7	23.6	N/A	1.3	N/A

To summarize this first part, it was demonstrated by NMR and XPS that a coating layer of oxide based aluminium was successfully deposited at the LNMO surface. SFCD process allows to obtain a better coverage than the dispersion method.

Electrochemical performance

Electrochemical properties were deeply characterized and analysed to demonstrate the influence of surface modification by an Al-rich coating on the electrochemical performance of LNMO, and to compare this performance depending on the process used to prepare the coating (Erreur ! Source du renvoi introuvable.**a-d**).
First, all the samples were evaluated as positive electrode materials versus Li metal at a low current rate of C/10, in the voltage range of 3.5 - 4.9 V vs Li^+/Li and at controlled temperature of 25 °C. Erreur ! Source du renvoi introuvable.**a** compares the results obtained for all the samples modified in supercritical conditions with the pristine material. It shows that the larger the content in Al-rich coating at the surface of LNMO, the smaller is the reversible gravimetric capacity. For instance, the SFCD 10 % sample exhibits only 88 $mAh.g^{-1}$ against 130 $mAh.g^{-1}$ for the SFCD 0.1 % sample and 135 $mAh.g^{-1}$ for the bare LNMO (**Figure 9d**). This result is expected as the coating is not electrochemically active. For the surface modified samples obtained by the dispersion process, the trend is the same as reported in **Figure S10** in supplementary information, except that for a similar expected content a larger gravimetric capacity is obtained (107 $mAh.g^{-1}$ for the DIS 10% sample vs 88 $mAh.g^{-1}$ for the SFCD 10% sample). This result also supports, as it was discussed previously, that the covering is thinner than expected with the dispersion process, and thus than that obtained by SFCD. After three formation cycles at C/10, all the samples were evaluated with a rate capability test showing increasing C-rates from C/10 (0.05 mA/cm^2) to 1C (0.50 mA/cm^2) or 4C (1.99 mA/cm^2) rate (charges in 10 h, 1 h, and 15 min, respectively) (**Figure 9b**). The main goal here is to estimate the impact of the coating on the fast charge performance. Small amount of coating improves the performance at fast rates but if the coating is too thick the performance decreases significantly. SFCD 0.5 % is the optimized sample. (Erreur ! Source du renvoi introuvable.**b)** Indeed, at low rates from C/10 to C/2 electrochemical performance is like those of the bare LNMO, while at higher rates (> C/2) better performance is obtained, especially at 4C. At the end of the rate capability test, the bare LNMO sample delivers a reversible capacity of 109 $mAh.g^{-1}$, which corresponds to 81.2 % of capacity retention, whereas the SFCD 0.5 % coated material shows 93.3 % of capacity retention

with still 119 mAh.g^{-1} delivered. It must be noted that despite mAh.g^{-1} corresponding to only 85.1 % of capacity retention,

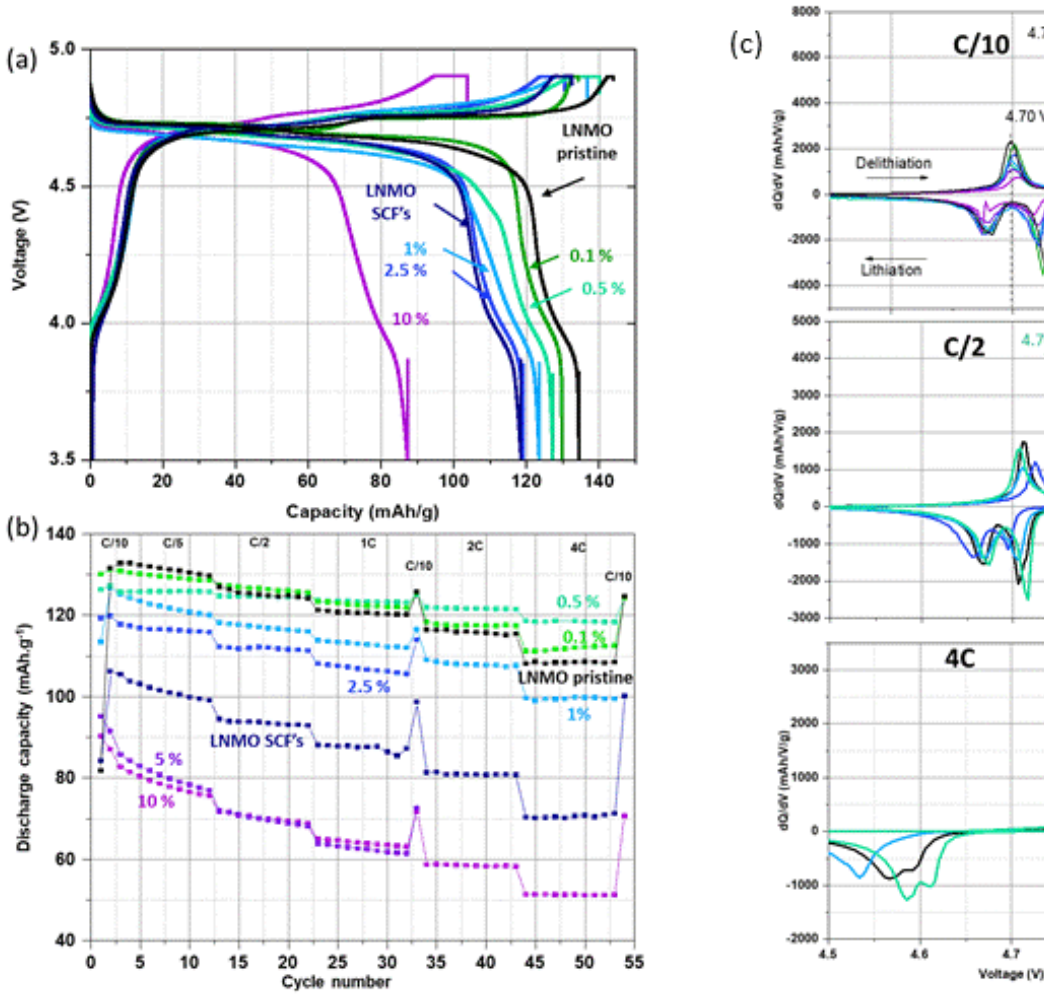

(d)

Material	Reversible capacity (mAh.g^{-1})
LNMO Pristine	135
LNMO SCFs	119
SFCD 0.1%	130
SFCD 0.5%	127
SFCD 1%	124
SFCD 2.5%	120
SFCD 10%	88

Figure 8 : Charge-discharge curves obtained for the 1st cycle at C/10 rate (a), rate capability tests from C/10 to 4C rates (b), dQ/dV curves obtained at different rates (C/10, C/2, 4C) (c) and comparison of reversible capacity obtained for each coated LNMO material at C/10 (d).

better performance versus the bare LNMO, the SFCD 0.1 % sample shows smaller improvement versus the SFCD 0.5 % sample, suggesting that the thickness of the coating has also to be optimized to reach optimized performance. In the case of the dispersion process, as the formation of the coating is less efficient, a larger theoretical content is necessary to significantly improve electrochemical performance. For the case of the dispersion coating, the DIS 1 % sample shows the best performance. Among all the samples compared, those modified by SCFD process show the best performance, despite the similar capacities values at low rates. They are significantly different at higher C-rate (2C, 4C). Indeed, DIS 1 % delivers 114 slightly better than for bare LNMO (81.2 %) but significantly smaller than for SFCD 0.5% (93.3 %).

dQ/dV curves give additional information about the redox activity. For LNMO, two different redox activities are observed: the first one in the voltage domain of 3.5 - 4.2 V vs. Li^+/Li is associated to the redox activity of manganese (Mn^{3+}/Mn^{4+}) and the second one in the voltage domain 4.4 - 4.9 V vs. Li^+/Li corresponds to nickel redox activity ($Ni^{2+}/Ni^{3+}/Ni^{4+}$). The broad shape of the first peak is characteristic of the solid solution domain, whereas the sharp shape of the two next oxidation peaks is characteristic of biphasic reactions. Erreur ! Source du

renvoi introuvable.**c** gives the comparison of the dQ/dV curves in nickel redox activity domain for bare and coated LNMO materials at C/10, C/2 and 4C, whereas a similar one in manganese redox activity domain is available in **Figure S11**. On the upper part of **Figure 9c**, at C/10, two peaks are observed as expected, at 4.70 and ~4.75 V vs. Li^+/Li in charge upon Li^+ delithiation from LNMO. The first peak corresponds to the Ni^{2+} to Ni^{3+} oxidation, and the second one to the Ni^{3+} to Ni^{4+} oxidation[34]. In the case of SFCD coated materials, these peaks are slightly shifted to higher voltages due to an increasing resistance associated to the Al-rich coating formed at the surface of the active material (as shown in **Figure S12** in supplementary information). **Table S5** gives a quantitative analysis of the redox processes involved depending on the thickness of the coating: the thicker it is, the less intense are the oxidation peaks revealing a decrease in nickel activity. The effect is even more pronounced for the second nickel redox activity (Ni^{3+}/Ni^{4+}). As a consequence, the intensity ratio between the Ni^{2+}/Ni^{3+} and the Ni^{3+}/Ni^{4+} redox peaks increase for thicker coating layers. When the cycling rate is increased to C/2, internal resistance tends to increase further the polarisation as shown by the shift of the oxidation peaks to even higher voltages (for the bare LNMO, 4.71 and 4.77 V at C/2 vs. 4.70 and 4.75 V at C/10). Finally, when the cycling rate is increased up to 4C the Ni^{3+}/Ni^{4+} redox activity almost disappears due to a strong polarisation, whereas that of the Ni^{2+}/Ni^{3+} redox couple is maintained. This behaviour is expected as the cycling rate increases. Nevertheless, it is interesting to highlight that the extent of the shift is mitigated for the SFCD 0.5 % sample, for which the coating would allow to mitigate the catalytic degradation of the electrolyte and thus the growth of the interface layer responsible for the internal resistance. Same trends are observed for the dispersion surface modified material.

For both processes, an optimum content of Al-rich coating was found to improve electrochemical performance versus those of the bare LNMO (SFCD 0.5 % and DIS 1 %).

Rate capability tests were performed (for these modified materials showing high performance (SFCD 0.5 % and DIS 1 %)) on high loading electrodes (11-12 mg/cm² vs. 3 mg/cm² for the previous results), in order to get closer to industrial loading and thus, to stress further the impact of the coating on electrochemical performance. Erreur ! Source du renvoi introuvable. shows the results obtained for a rate capability test with increasing C-rates from C/10 to 4C. The beneficial impact of the coating appears even more pronounced in the case of higher loading electrodes. Indeed, at 4C, SFCD 0.5 % delivers the best specific capacity with 86 mAh/g versus only 23 and 16 mAh/g for DIS 1 % and bare LNMO, respectively. Thus, the coating done by SFCD permits to stabilize the material at high rates. A comparison of the obtained performance, between the two loadings used 3 mg/cm² and 12 mg/cm², was done in **Figure S13** for the coated sample SFCD 0.5%.

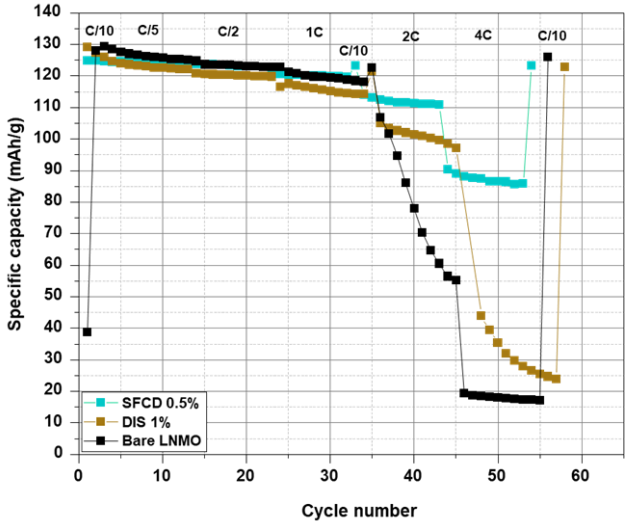

Figure 9 : Rate capability tests with increasing rates from C/10 to 4C for highly loaded electrodes (12 mg/cm²), for bare LNMO and for the best performance materials modified by dispersion and SFCD processes.

In order to check for the phase stability after cycling at high C-rate, post mortem analyses were performed after 100 cycles at 4C, a charge at C/10 and then a discharge at C/10 down to 3.5 V vs. Li^+/Li until current reaches a steady state close to 0 mA. XRD patterns were collected after disassembling the cell in a glovebox under argon, washing the electrode in an excess of dried DMC and preparing a sample-holder under argon (**Figure S14** showing XRD patterns and Le Bail refinements after cycling (a-b), lattice parameters (c), SEM pictures (d-e**)**). Each XRD pattern was refined considering a single phase described as the pristine spinel phase in the *Fd-3m* space group. A slight change (decrease) in cell parameters is observed, but it is expected as the recovered materials are not fully lithiated after this long cycling at high rate: 8.1698(2) and 8.1694(2) Å for SFCD 0.5 % and DIS 1 %, respectively, versus 8.1714(4) Å for the pristine LNMO. These smaller lattice parameters are in good agreement with a higher average oxidation state for the transition metal ions within the structure, and thus a smaller Li^+ re-intercalation ratio. As shown by similar FWHM values ($FWHM_{(111)\ SFCD}$ = 0.0937(14) °and $FWHM_{(111)\ DIS}$ = 0.0932(14) °vs $FWHM_{(111)\ LNMO}$ = 0.1154(3) °), no modification of the crystalline size domain is observed upon cycling. SEM images were done on post cycling materials and the morphology was not altered by fast charge. Improvement of electrochemical performance at high rates was demonstrated for coated materials (SFCD 0.5 % and DIS 1 %), even for high loaded electrodes, and SFCD coated material revealed better stabilization at high rate than dispersion coated material. These results clearly appear attractive/competitive versus/with those reported in literature[14–16,29–31,58,59] (Erreur ! Source du renvoi introuvable.), despite the difficulties to compare them directly because of lack of information on the C-rate, loading, formulation, electrolyte ….

Table 2 : Summary of results reported in literature for Al_2O_3 modified LNMO materials used at the positive electrode of half cells versus Li metal

Coating technique	Electrode loading (mg/cm²)	Rate capability at 25°C (mAh/g)$	Cycling test at 25°C (mAh/g)	Number of cycles	Reference
ALD (electrode)	na	92 (5C)	118 (C/2 CCCV)	200	[29]
ALD (electrode)	na	na*	105 (C/2) (CC)	200	[30]
ALD (electrode)	na	na	122 (C/2) (CCCV)	100	[31]
Sol gel	na	76 (2C)	99 (1C na)	100	[58]
Coprecipitation	na	105 (20C discharge)	124 (1C) (CC)	300	[59]
Coprecipitation	na	na	134 (C/2 na)	100	[16]
Wet technique	2.85	100 (20C discharge)	120 (C/2 CC)	200	[15]
Wet technique	1.1	83 (7C)	118 (1C CC)	200	[14]
Dispersion	3	114 (4C)	na	na	*This work*
SFCD	3	119 (4C)	na	na	*This work*
Dispersion	12	24 (4C)	na	na	*This work*
SFCD	12	86 (4C)	na	na	*This work*

*not available

$The capacity given in the table is the one obtained at the higher cycling rate

CONCLUSIONS

The formation of Al_2O_3-type coating was investigated by two techniques: dispersion, a conventional route, and supercritical fluid chemical deposition, never used in the field of battery materials. SFCD is an up-scalable and sustainable promising process. A coating could be deposited at the surface of commercial LNMO particles. The formation of a more continuous and homogeneous coating versus that obtained by dispersion process was demonstrated by combining complementary spectroscopic analyses (NMR, XPS and nano Auger). The SFCD modified LNMO with 0.5% of Al-rich coating, estimated to be about 3 nm in thickness, revealed very attractive performance at high cycling rates (> 2C), even for highly loaded electrodes. Indeed, a reversible capacity of ~120 $mAh.g^{-1}$ is maintained at 4C. This protected LNMO material could be also of interest for more challenging batteries such as all solid-state batteries that require controlling reactivity at interfaces between the electrodes and the electrolyte. Beyond LNMO, SFCD appears as a process to explore widely to tune the nature of protective interfacial layers used to modify both the electrodes and the electrolytes.

Conflicts of interest

There are no conflicts to declare.

Supporting Information

The Supporting Information contains more Figures, Tables and some description to complete and precise some points in the main manuscript, such as : TGA $Al(acac)_3$, chemical analyses performed by ICP-OES; refined patterns and parameters obtained by Le Bail refinements; XRD patterns of the degraded precursors by both processes: dispersion and SFCD; ^{7}Li MAS NMR spectra for coated and uncoated materials and ^{27}Al MAS NMR spectra for the reference materials obtained by both processes; Raman and FT-IR extended range spectra obtained for coated materials with assignments; XPS survey and quantifications; electrochemical performance obtained for the coated materials obtained by dispersion process; dQ/dV curves for the manganese associated voltage domain and the post mortem analyses realised by SEM and XRD.

Acknowledgements

The authors acknowledge ANRT, Renault SAS and Région Nouvelle-Aquitaine for the funding of the project, ANRT and Renault SAS for the funding (CIFRE grant) of G. C.'s PhD thesis, as well as the French National Research Agency (STORE-EX Labex Project ANR-10-LABX-76-01) for financial support for

their research on the electrochemical energy storage. The authors would like also to acknowledge Nano One Materials Corp for providing the LNMO material used for the project. The authors thank Guillaume Aubert, Cathy Denage, Jérôme Kalisky and Eric Lebraud at ICMCB for their technical support for SCFD process, ICP-OES, SEM and XRD, respectively. The authors also thank Philippe Legros, Marion Gayot, Mélanie Vaudescal and Nithavong Cam at PLACAMAT and François Weill at ICMCB for their scientific support with SEM and Nano Auger analyses.

References

(1) Tarascon, J.-M.; Armand, M. Issues and Challenges Facing Rechargeable Lithium Batteries. *Nature* **2001**, *414* (6861), 359–367. https://doi.org/10.1038/35104644.

(2) Knobloch, F.; Hanssen, S. V.; Lam, A.; Pollitt, H.; Salas, P.; Chewpreecha, U.; Huijbregts, M. A. J.; Mercure, J.-F. Net Emission Reductions from Electric Cars and Heat Pumps in 59 World Regions over Time. *Nat. Sustain.* **2020**, *3* (6), 437–447. https://doi.org/10.1038/s41893-020-0488-7.

(3) Noh, H.-J.; Youn, S.; Yoon, C. S.; Sun, Y.-K. Comparison of the Structural and Electrochemical Properties of Layered Li[NixCoyMnz]O2 (x = 1/3, 0.5, 0.6, 0.7, 0.8 and 0.85) Cathode Material for Lithium-Ion Batteries. *J. Power Sources* **2013**, *233*, 121–130. https://doi.org/10.1016/j.jpowsour.2013.01.063.

(4) Chen, C. H.; Liu, J.; Stoll, M. E.; Henriksen, G.; Vissers, D. R.; Amine, K. Aluminum-Doped Lithium Nickel Cobalt Oxide Electrodes for High-Power Lithium-Ion Batteries. *J. Power Sources* **2004**, *128* (2), 278–285. https://doi.org/10.1016/j.jpowsour.2003.10.009.

(5) Croguennec, L.; Palacin, M. R. Recent Achievements on Inorganic Electrode Materials for Lithium-Ion Batteries. *J. Am. Chem. Soc.* **2015**, *137* (9), 3140–3156. https://doi.org/10.1021/ja507828x.

(6) *London Metal Exchange*. https://www.lme.com/Metals/EV/LME-Cobalt#Price+graphs.

(7) Goodenough, J. B.; Kim, Y. Challenges for Rechargeable Li Batteries. *Chem. Mater.* **2010**, *22* (3), 587–603. https://doi.org/10.1021/cm901452z.

(8) Harris, O. C.; Lee, S. E.; Lees, C.; Tang, M. Review: Mechanisms and Consequences of Chemical Cross-Talk in Advanced Li-Ion Batteries. *J. Phys. Energy* **2020**, *2* (3), 032002. https://doi.org/10.1088/2515-7655/ab8b68.

(9) Fan, X.; Wang, C. High-Voltage Liquid Electrolytes for Li Batteries: Progress and Perspectives. *Chem. Soc. Rev.* **2021**, *50* (18), 10486–10566. https://doi.org/10.1039/D1CS00450F.

(10) Dong, Y.; Young, B. T.; Zhang, Y.; Yoon, T.; Heskett, D. R.; Hu, Y.; Lucht, B. L. Effect of Lithium Borate Additives on Cathode Film Formation in $LiNi_{0.5}Mn_{1.5}O_4$/Li Cells. *ACS Appl. Mater. Interfaces* **2017**, *9* (24), 20467–20475. https://doi.org/10.1021/acsami.7b01481.

(11) Hofmann, A.; Höweling, A.; Bohn, N.; Müller, M.; Binder, J. R.; Hanemann, T. Additives for Cycle Life Improvement of High-Voltage LNMO-Based Li-Ion Cells. *ChemElectroChem* **2019**, *6* (20), 5255–5263. https://doi.org/10.1002/celc.201901120.

(12) Kim, J. W.; Kim, D. H.; Oh, D. Y.; Lee, H.; Kim, J. H.; Lee, J. H.; Jung, Y. S. Surface Chemistry of LiNi0.5Mn1.5O4 Particles Coated by Al2O3 Using Atomic Layer Deposition for Lithium-Ion Batteries. *J. Power Sources* **2015**, *274*, 1254–1262. https://doi.org/10.1016/j.jpowsour.2014.10.207.

(13) Sun, P.; Ma, Y.; Zhai, T.; Li, H. High Performance LiNi0.5Mn1.5O4 Cathode by Al-Coating and Al3+-Doping through a Physical Vapor Deposition Method. *Electrochim Acta* **2016**, *191*, 237–246. https://doi.org/10.1016/j.electacta.2016.01.087.

(14) Chang, Q.; Wei, A.; Li, W.; Bai, X.; Zhang, L.; He, R.; Liu, Z. Structural and Electrochemical Characteristics of Al2O3-Modified LiNi0.5Mn1.5O4 Cathode Materials for Lithium-Ion Batteries. *Ceram. Int.* **2019**, *45* (4), 5100–5110. https://doi.org/10.1016/j.ceramint.2018.11.213.

(15) Shu, Y.; Xie, Y.; Yan, W.; Meng, S.; Sun, D.; Jin, Y.; Xiang, L. Tuning the Ratio of Al2O3 to LiAlO2 in the Composite Coating Layer for High Performance LiNi0.5Mn1.5O4 Materials. *Ceram. Int.* **2020**, *46* (10), 14840–14846. https://doi.org/10.1016/j.ceramint.2020.03.009.

(16) Li, S.; Liang, W.; Xie, J.; Wei, Y.; Cui, X. Synthesis of Hollow Microspheres LiNi0.5Mn1.5O4 Coated With Al2O3 and Characterization of the Electrochemical Capabilities. *J. Electrochem. Energy Convers. Storage* **2020**, *17* (3). https://doi.org/10.1115/1.4045566.

(17) Ma, C.; Wen, Y.; Qiao, Q.; He, P.; Ren, S.; Li, M.; Zhao, P.; Qiu, J.; Tang, G. Improving Electrochemical Performance of High-Voltage Spinel $LiNi_{0.5}Mn_{1.5}O_4$ Cathodes by Silicon Oxide Surface Modification. *ACS Appl. Energy Mater.* **2021**, *4* (11), 12201–12210. https://doi.org/10.1021/acsaem.1c01891.

(18) Zhao, J.; Liu, Y.; He, Y.; Lu, K. Li4Ti5O12 Epitaxial Coating on LiNi0.5Mn1.5O4 Surface for Improving the Electrochemical Performance through Solvothermal-Assisted Processing. *J. Alloys Compd.* **2019**, *779*, 978–984. https://doi.org/10.1016/j.jallcom.2018.11.152.

(19) Liu, J.; Manthiram, A. Improved Electrochemical Performance of the 5 V Spinel Cathode LiMn[Sub 1.5]Ni[Sub 0.42]Zn[Sub 0.08]O[Sub 4] by Surface Modification. *J. Electrochem. Soc.* **2009**, *156* (1), A66. https://doi.org/10.1149/1.3028318.

(20) Wu, Q.; Yin, Y.; Sun, S.; Zhang, X.; Wan, N.; Bai, Y. Novel AlF3 Surface Modified Spinel LiMn1.5Ni0.5O4 for Lithium-Ion Batteries: Performance Characterization and Mechanism Exploration. *Electrochim Acta* **2015**, *158*, 73–80. https://doi.org/10.1016/j.electacta.2015.01.145.

(21) Shapira, A.; Tiurin, O.; Solomatin, N.; Auinat, M.; Meitav, A.; Ein-Eli, Y. Robust AlF_3 Atomic Layer Deposition Protective Coating on $LiMn_{1.5}Ni_{0.5}O_4$ Particles: An Advanced Li-Ion Battery Cathode Material Powder. *ACS Appl. Energy Mater.* **2018**, *1* (12), 6809–6823. https://doi.org/10.1021/acsaem.8b01048.

(22) Li, Y.; Zhang, Q.; Xu, T.; Wang, D.; Pan, D.; Zhao, H.; Bai, Y. LaF3 Nanolayer Surface Modified Spinel LiNi0.5Mn1.5O4 Cathode Material for Advanced Lithium-Ion Batteries. *Ceram. Int.* **2018**, *44* (4), 4058–4066. https://doi.org/10.1016/j.ceramint.2017.11.203.

(23) Li, L.; Zhao, R.; Xu, T.; Wang, D.; Pan, D.; Zhang, K.; Yu, C.; Lu, X.; He, G.; Bai, Y. Stabilizing a High-Voltage $LiNi_{0.5}Mn_{1.5}O_4$ Cathode towards All Solid State Batteries: A Li–Al–Ti–P–O Solid Electrolyte Nano-Shell with a Host Material. *Nanoscale* **2019**, *11* (18), 8967–8977. https://doi.org/10.1039/C9NR01655D.

(24) College of Physics and Electronic Information, Inner Mongolia Normal University, Hohhot 010022, China.; Wu, D. Solid Electrolyte Li1.4Al0.4Ti1.6(PO4)3 as Coating for High Voltage Spinel LiNi0.5Mn1.5O4 Cathode Material. *Int. J. Electrochem. Sci.* **2020**, 3715–3728. https://doi.org/10.20964/2020.05.35.

(25) Myung, S.-T.; Izumi, K.; Komaba, S.; Yashiro, H.; Bang, H. J.; Sun, Y.-K.; Kumagai, N. Functionality of Oxide Coating for $Li[Li_{0.05}Ni_{0.4}Co_{0.15}Mn_{0.4}]O_2$ as Positive Electrode Materials for Lithium-Ion Secondary Batteries. *J. Phys. Chem. C* **2007**, *111* (10), 4061–4067. https://doi.org/10.1021/jp0674367.

(26) Myung, S.-T.; Izumi, K.; Komaba, S.; Sun, Y.-K.; Yashiro, H.; Kumagai, N. Role of Alumina Coating on Li−Ni−Co−Mn−O Particles as Positive Electrode Material for Lithium-Ion Batteries. *Chem. Mater.* **2005**, *17* (14), 3695–3704. https://doi.org/10.1021/cm050566s.

(27) Oh, Y.; Ahn, D.; Nam, S.; Park, B. The Effect of Al2O3-Coating Coverage on the Electrochemical Properties in LiCoO2 Thin Films. *J. Solid State Electrochem.* **2010**, *14* (7), 1235–1240. https://doi.org/10.1007/s10008-009-0946-7.

(28) Jurng, S.; Heiskanen, S. K.; Chandrasiri, K. W. D. K.; Abeywardana, M. Y.; Lucht, B. L. Minimized Metal Dissolution from High-Energy Nickel Cobalt Manganese Oxide Cathodes with Al_2O_3 Coating and Its Effects on Electrolyte Decomposition on Graphite Anodes. *J. Electrochem. Soc.* **2019**, *166* (13), A2721–A2726. https://doi.org/10.1149/2.0101913jes.

(29) Fang, X.; Ge, M.; Rong, J.; Che, Y.; Aroonyadet, N.; Wang, X.; Liu, Y.; Zhang, A.; Zhou, C. Ultrathin Surface Modification by Atomic Layer Deposition on High Voltage Cathode $LiNi_{0.5}Mn_{1.5}O_4$ for Lithium Ion Batteries. *Energy Technol.* **2014**, *2* (2), 159–165. https://doi.org/10.1002/ente.201300102.

(30) Song, J.; Han, X.; Gaskell, K. J.; Xu, K.; Lee, S. B.; Hu, L. Enhanced Electrochemical Stability of High-Voltage LiNi0.5Mn1.5O4 Cathode by Surface Modification Using Atomic Layer Deposition. *J. Nanoparticle Res.* **2014**, *16* (11). https://doi.org/10.1007/s11051-014-2745-z.

(31) Fang, X.; Lin, F.; Nordlund, D.; Mecklenburg, M.; Ge, M.; Rong, J.; Zhang, A.; Shen, C.; Liu, Y.; Cao, Y.; Doeff, M. M.; Zhou, C. Atomic Insights into the Enhanced Surface Stability in High Voltage Cathode Materials by Ultrathin Coating. *Adv. Funct. Mater.* **2017**, *27* (7), 1602873. https://doi.org/10.1002/adfm.201602873.

(32) Li, W.; Cheng, D.; Shimizu, R.; Li, Y.; Yao, W.; Raghavendran, G.; Zhang, M.; Meng, Y. S. Artificial Cathode Electrolyte Interphase for Improving High Voltage Cycling Stability of Thick Electrode with Co-Free 5 V Spinel Oxides. *Energy Storage Mater.* **2022**, *49*, 77–84. https://doi.org/10.1016/j.ensm.2022.04.002.

(33) Johnson, R. W.; Hultqvist, A.; Bent, S. F. A Brief Review of Atomic Layer Deposition: From Fundamentals to Applications. *Mater. Today* **2014**, *17* (5), 236–246. https://doi.org/10.1016/j.mattod.2014.04.026.

(34) Liang, G.; Peterson, V. K.; See, K. W.; Guo, Z.; Pang, W. K. Developing High-Voltage Spinel $LiNi_{0.5}Mn_{1.5}O_4$ Cathodes for High-Energy-Density Lithium-Ion Batteries: Current Achievements and Future Prospects. *J. Mater. Chem. A* **2020**, *8* (31), 15373–15398. https://doi.org/10.1039/D0TA02812F.

(35) Qureshi, Z. A.; Tariq, H. A.; Shakoor, R. A.; Kahraman, R.; AlQaradawi, S. Impact of Coatings on the Electrochemical Performance of LiNi0.5Mn1.5O4 Cathode Materials: A Focused Review. *Ceram. Int.* **2022**, *48* (6), 7374–7392. https://doi.org/10.1016/j.ceramint.2021.12.118.

(36) Nisar, U.; Muralidharan, N.; Essehli, R.; Amin, R.; Belharouak, I. Valuation of Surface Coatings in High-Energy Density Lithium-Ion Battery Cathode Materials. *Energy Storage Mater.* **2021**, *38*, 309–328. https://doi.org/10.1016/j.ensm.2021.03.015.

(37) Aymonier, C.; Elissalde, C.; Reveron, H.; Weill, F.; Maglione, M.; Cansell, F. Supercritical Fluid Technology of Nanoparticle Coating for New Ceramic Materials. *J. Nanosci. Nanotechnol.* **2005**, *5* (6), 980–983. https://doi.org/10.1166/jnn.2005.147.

(38) Majimel, M.; Marre, S.; Garrido, E.; Aymonier, C. Supercritical Fluid Chemical Deposition as an Alternative Process to CVD for the Surface Modification of Materials. *Chem. Vap. Depos.* **2011**, *17* (10–12), 342–352. https://doi.org/10.1002/cvde.201106921.

(39) Campalani, C.; Amadio, E.; Zanini, S.; Dall'Acqua, S.; Panozzo, M.; Ferrari, S.; De Nadai, G.; Francescato, S.; Selva, M.; Perosa, A. Supercritical CO2 as a Green Solvent for the Circular Economy: Extraction of Fatty Acids from Fruit Pomace. *J. CO2 Util.* **2020**, *41*, 101259. https://doi.org/10.1016/j.jcou.2020.101259.

(40) Oviroh, P. O.; Akbarzadeh, R.; Pan, D.; Coetzee, R. A. M.; Jen, T.-C. New Development of Atomic Layer Deposition: Processes, Methods and Applications. *Sci. Technol. Adv. Mater.* **2019**, *20* (1), 465–496. https://doi.org/10.1080/14686996.2019.1599694.

(41) Aymonier, C.; Philippot, G.; Erriguible, A.; Marre, S. Playing with Chemistry in Supercritical Solvents and the Associated Technologies for Advanced Materials by Design. *J. Supercrit. Fluids* **2018**, *134*, 184–196. https://doi.org/10.1016/j.supflu.2017.12.021.

(42) Pöhler, H.; Kiran, E. Volumetric Properties of Carbon Dioxide + Ethanol at High Pressures. *J. Chem. Eng. Data* **1997**, *42* (2), 384–388. https://doi.org/10.1021/je9602982.

(43) Rodríguez-Carvajal, J. Recent Advances in Magnetic Structure Determination by Neutron Powder Diffraction. *Phys. B Condens. Matter* **1993**, *192* (1–2), 55–69. https://doi.org/10.1016/0921-4526(93)90108-I.

(44) Chemelewski, K. R.; Shin, D. W.; Li, W.; Manthiram, A. Octahedral and Truncated High-Voltage Spinel Cathodes: The Role of Morphology and Surface Planes in Electrochemical Properties. *J. Mater. Chem. A* **2013**, *1* (10), 3347. https://doi.org/10.1039/c3ta00682d.

(45) Cui, J.; Kast, M. G.; Hammann, B. A.; Afriyie, Y.; Woods, K. N.; Plassmeyer, P. N.; Perkins, C. K.; Ma, Z. L.; Keszler, D. A.; Page, C. J.; Boettcher, S. W.; Hayes, S. E. Aluminum Oxide Thin Films from Aqueous Solutions: Insights from Solid-State NMR and Dielectric Response. *Chem. Mater.* **2018**, *30* (21), 7456–7463. https://doi.org/10.1021/acs.chemmater.7b05078.

(46) Kwak, J.; Hu, J.; Kim, D.; Szanyi, J.; Peden, C. Penta-Coordinated Al3+ Ions as Preferential Nucleation Sites for BaO on γ-Al2O3: An Ultra-High-Magnetic Field 27Al MAS NMR Study. *J. Catal.* **2007**, *251* (1), 189–194. https://doi.org/10.1016/j.jcat.2007.06.029.

(47) Lee, S. K.; Ahn, C. W. Probing of 2 Dimensional Confinement-Induced Structural Transitions in Amorphous Oxide Thin Film. *Sci. Rep.* **2015**, *4* (1). https://doi.org/10.1038/srep04200.

(48) Lee, S. K.; Park, S. Y.; Yi, Y. S.; Moon, J. Structure and Disorder in Amorphous Alumina Thin Films: Insights from High-Resolution Solid-State NMR. *J. Phys. Chem. C* **2010**, *114* (32), 13890–13894. https://doi.org/10.1021/jp105306r.

(49) Kim, J.-H.; Huq, A.; Chi, M.; Pieczonka, N. P. W.; Lee, E.; Bridges, C. A.; Tessema, M. M.; Manthiram, A.; Persson, K. A.; Powell, B. R. Integrated Nano-Domains of Disordered and Ordered Spinel Phases in $LiNi_{0.5}Mn_{1.5}O_4$ for Li-Ion Batteries. *Chem. Mater.* **2014**, *26* (15), 4377–4386. https://doi.org/10.1021/cm501203r.

(50) Battaglin, F. A. D.; Prado, E. S.; Caseli, L.; Silva, T. F. da; Tabacniks, M. H.; Cruz, N. C. da; Rangel, E. C. Films Deposited from Reactive Sputtering of Aluminum Acetylacetonate Under Low Energy Ion Bombardment. *Mater. Res.* **2017**, *20* (4), 926–936. https://doi.org/10.1590/1980-5373-mr-2016-0647.

(51) Schmidt, B. W.; Rogers, B. R.; Gren, C. K.; Hanusa, T. P. Carbon Incorporation in Chemical Vapor Deposited Aluminum Oxide Films. *Thin Solid Films* **2010**, *518* (14), 3658–3663. https://doi.org/10.1016/j.tsf.2009.09.105.

(52) Stranick, M. A. MnO2 by XPS. *Surf. Sci. Spectra* **1999**, *6* (1), 31–38. https://doi.org/10.1116/1.1247888.

(53) Wei, Y.; Kim, K.-B.; Chen, G. Evolution of the Local Structure and Electrochemical Properties of Spinel LiNixMn2−xO4 (0≤x≤0.5). *Electrochim Acta* **2006**, *51* (16), 3365–3373. https://doi.org/10.1016/j.electacta.2005.09.035.
(54) Biesinger, M. C.; Lau, L. W. M.; Gerson, A. R.; Smart, R. St. C. The Role of the Auger Parameter in XPS Studies of Nickel Metal, Halides and Oxides. *Phys. Chem. Chem. Phys.* **2012**, *14* (7), 2434. https://doi.org/10.1039/c2cp22419d.
(55) Østli, E. R.; Tesfamhret, Y.; Wenner, S.; Lacey, M. J.; Brandell, D.; Svensson, A. M.; Selbach, S. M.; Wagner, N. P. Limitations of Ultrathin Al_2O_3 Coatings on LNMO Cathodes. *ACS Omega* **2021**, *6* (45), 30644–30655. https://doi.org/10.1021/acsomega.1c04457.
(56) Kloprogge, J. T.; Duong, L. V.; Wood, B. J.; Frost, R. L. XPS Study of the Major Minerals in Bauxite: Gibbsite, Bayerite and (Pseudo-)Boehmite. *J. Colloid Interface Sci.* **2006**, *296* (2), 572–576. https://doi.org/10.1016/j.jcis.2005.09.054.
(57) Hwang, T.; Lee, J. K.; Mun, J.; Choi, W. Surface-Modified Carbon Nanotube Coating on High-Voltage LiNi0.5Mn1.5O4 Cathodes for Lithium Ion Batteries. *J. Power Sources* **2016**, *322*, 40–48. https://doi.org/10.1016/j.jpowsour.2016.04.118.
(58) Huang, X.; Chen, K.; Liu, Y. Enhancement of $LiNi_{0.5}Mn_{1.5}O_4$ Cathode Materials through Interfacial Modification of Amorphous Al_2O_3 in Lithium Ion Batteries. *J. Electrochem. Soc.* **2019**, *166* (3), A5081–A5089. https://doi.org/10.1149/2.0141903jes.
(59) Song, C.; Lu, J.; Liu, Y.; Yuan, Q.; Yang, J.; He, H.; Liu, D.; Wang, Q. Enhanced Electrochemical Performance of Spinel LiNi0.5Mn1.5O4 for Li-Ion Batteries with Moderate Mn3+ Concentration and Nanosized Thin Al2O3 Coating. *J. Mater. Sci. Mater. Electron.* **2020**, *31* (6), 4815–4821. https://doi.org/10.1007/s10854-020-03043-0.